



**HAL**  
open science

# The role of surface states and point defects on optical properties of InGaN/GaN multi-quantum wells in nanowires grown by molecular beam epitaxy

Alexandre Concordel, Joël Bleuse, Gwénoél Jacopin, Bruno Daudin

## ► To cite this version:

Alexandre Concordel, Joël Bleuse, Gwénoél Jacopin, Bruno Daudin. The role of surface states and point defects on optical properties of InGaN/GaN multi-quantum wells in nanowires grown by molecular beam epitaxy. *Nanotechnology*, 2022, 34 (3), pp.035703. 10.1088/1361-6528/ac98cd. hal-03864814

**HAL Id: hal-03864814**

**<https://hal.science/hal-03864814v1>**

Submitted on 10 Oct 2023

**HAL** is a multi-disciplinary open access archive for the deposit and dissemination of scientific research documents, whether they are published or not. The documents may come from teaching and research institutions in France or abroad, or from public or private research centers.

L'archive ouverte pluridisciplinaire **HAL**, est destinée au dépôt et à la diffusion de documents scientifiques de niveau recherche, publiés ou non, émanant des établissements d'enseignement et de recherche français ou étrangers, des laboratoires publics ou privés.

# The role of surface states and point defects on optical properties of InGaN/GaN multi-quantum wells in nanowires grown by molecular beam epitaxy

Alexandre Concordel<sup>1</sup>, Joël Bleuse<sup>1</sup>, Gwénoél Jacopin<sup>2</sup> and Bruno Daudin<sup>1</sup>

<sup>1</sup>Université Grenoble Alpes, CEA, IRIG, F-38000 Grenoble, France

<sup>2</sup>Univ. Grenoble Alpes, CNRS, Grenoble INP, Institut Néel, 38000 Grenoble, France

Corresponding author: [alexandre.concordel@cea.fr](mailto:alexandre.concordel@cea.fr)

## ABSTRACT

The optical properties of nanowire-based InGaN/GaN multiple quantum wells (MQWs) heterostructures grown by plasma-assisted molecular beam epitaxy are investigated. The beneficial effect of an InGaN underlayer grown below the active region is demonstrated and assigned to the trapping of point defects transferred from the pseudo-template to the active region. The influence of surface recombination is also investigated. We demonstrate an efficient surface passivation thanks to AlO<sub>x</sub> deposition for low InN molar fraction value. By contrast, for large InN molar fraction, the surface recombination is masked by an increased non-radiative recombination, assigned to the formation of additional point defects during the growth of InGaN/GaN multiple quantum wells heterostructure. The inhomogeneous luminescence of single nanowires at the nanoscale, namely a luminescent ring surrounding a less luminescent centre part points towards an inhomogeneous spatial distribution of the non-radiative recombination centers (NRCs) tentatively identified to intrinsic point defects created during the MQWs growth.

**KEYWORDS:** InGaN, nanowire, LED, luminescence efficiency, recombination dynamics, Molecular Beam Epitaxy, Cathodoluminescence

## 1. INTRODUCTION

Since decades, III-Nitride materials are a subject of continuous basic and technological research because of their light emission properties in a wavelength range that spans from ultraviolet (UV) to infrared (IR). These sustained efforts have culminated with the realization of violet-blue light-emitting diodes (LEDs) exhibiting an internal quantum efficiency (IQE) of more than 90%<sup>1</sup>. More recently, III-Nitrides materials have become a central focus of research to develop microLEDs.<sup>2-5</sup> Particularly, InGaN/GaN MQWs-based heterostructures were demonstrated as lighting and display sources since they cover the full visible emission range<sup>6</sup>. However, the performances of native color InGaN/GaN microdisplays still need to be improved. Indeed, the growth of InGaN presents a number of challenging issues that limit the IQE of active layers, particularly in the yellow-red range<sup>7</sup>. This decreasing IQE for increasing InN molar fraction is partly assigned to the degradation of the material structural and optical quality caused by the relaxation of the built-up strain in MQWs, because of an increasing InGaN/GaN lattice mismatch together with an increasing influence of the quantum confined Stark effect. This contributes to the IQE drop at long wavelength emission.

Recent researches focused on the elaboration of nanowires (NWs) based microLEDs<sup>8-10</sup>. Indeed, for a diameter small enough<sup>11,12</sup>, the high aspect ratio of NWs allows one to grow heterostructures that are free of extended defects such as dislocations<sup>13-16</sup>, which are known to act as significant non-radiative recombination centres (NRCs)<sup>17,18</sup> especially for a density above  $10^8 \text{ cm}^{-2}$ . However, as a counterpart, this high surface/volume ratio and the presence of surface states potentially favours non-radiative surface recombinations.<sup>19,20</sup> Besides, the influence of point defects, also responsible for reducing the luminescence efficiency of the emitting layers should equally affect NW heterostructures. In fact, point defect incorporation is intrinsically related to growth conditions. Whatever the growth technique, residual impurities incorporation is one source. Such impurities may act as exciton trapping centres, resulting in parasitic

luminescence or non-radiative recombinations. In addition, the thermodynamically-driven formation of N or Ga vacancies ( $V_N$ ,  $V_{Ga}$ ) is another source of point defects, directly linked to growth temperature and metal/N species ratios.  $V_{Ga}$  forming complexes with other point defects are known to act as NRCs, leading to a decrease in luminescence efficiency and shorter recombination lifetime<sup>21,22</sup>. A special attention was recently paid to the case of  $V_N$ . In particular, it was found that the addition of an InGaN underlayer (UL) grown before the MQWs in InGaN/GaN layered heterostructures elaborated by metalorganic vapour phase deposition (MOCVD) led to a marked improvement of luminescence<sup>23-27</sup>. This effect was tentatively assigned to the ability of this UL, containing a low In content, to trap  $V_N$  forming at the GaN surface.<sup>24</sup> Due to their chemical affinity with In atoms<sup>28,29</sup>,  $V_N$  are incorporated and trapped inside the InGaN UL by creating complexes with In atoms. Hence, as a consequence of the reduced surface defect density, a significant increase of the luminescence efficiency of layered LEDs is observed. However, the impact of such an UL in InGaN/GaN NW heterostructures elaborated by Plasma Assisted Molecular Beam Epitaxy (PA-MBE) at growth temperatures lower than in MOCVD still remains to be investigated.

Using a combination of optical characterization techniques, we highlight the impact of an InGaN UL grown before the QWs on the luminescence efficiency of InGaN/GaN NW heterostructures elaborated by PA-MBE. We also demonstrate the importance of a surface passivation step to avoid surface recombination and show that the surface recombination influence decreases when the InN molar fraction in the QWs increases while the role of other NRCs becomes prominent, associated with luminescence inhomogeneities at the nanoscale.

## 2. EXPERIMENTAL SECTION

The pseudo-templates used in this work consist of ordered arrays of MOCVD-grown GaN NWs elaborated by selective area growth (SAG) on a sapphire substrate covered by a 5  $\mu\text{m}$ , Ga-polar n-doped GaN buffer layer. Prior to the growth, a 40 nm SiN mask is deposited by low pressure chemical vapor deposition, and patterned by e-beam lithography, to realize homogeneous arrays of holes with different diameters. Then, GaN NWs are grown from these holes. Non-negligible lateral growth enlarges the NWs, leading to final diameters that range from 135 nm to 280 nm. The NWs spacing is 400 nm. Following introduction in the PA-MBE growth chamber, these pseudo-templates are outgassed at 950°C during 45 min before further deposition of the MBE-grown section. The list of the samples investigated in this work is displayed in Table 1. Sample A, B and C emitting respectively at 480 nm, 590 nm and 615 nm, are composed of a 25-nm thick GaN layer, deposited on the pseudo-template, followed by the growth of a nominally 50 nm thick InGaN UL with an In content of about 3% and a 20-nm thick GaN spacer. The emitting region consisted in  $\text{In}_{0.15}\text{Ga}_{0.85}\text{N}/\text{GaN}$ ,  $\text{In}_{0.29}\text{Ga}_{0.71}\text{N}/\text{GaN}$  and  $\text{In}_{0.32}\text{Ga}_{0.68}\text{N}/\text{GaN}$  MQWs, respectively. The structure of sample D, emitting at 480 nm, is similar to sample A. However, sample D differed from sample A by a slower growth rate of 0.14 ML/s for the emitting region (0.37 ML/s for sample A). Finally, a 3 nm thick GaN capping layer was deposited to encapsulate the MQW structure, before an annealing step of 20 min at 900°C. Samples A' and B' were obtained by the additional deposition of an aluminium oxide ( $\text{AlO}_x$ ) layer on sample A and B, respectively. Such an  $\text{AlO}_x$  passivation layer was also deposited on sample D. In the reference sample without UL, an additional GaN layer of same thickness was grown in order to maintain constant for all samples the total thickness of the section overgrown by MBE on the template before growth of the MQW section.

Sample	InGaN underlayer	AlO <sub>x</sub> deposition	QW Emission wavelength <sup>[gj1]</sup>
Reference	No	No	480 nm
A	Yes	No	480 nm
A'	Yes	Yes	480 nm
B	Yes	No	590 nm
B'	Yes	Yes	590 nm
C	Yes	No	615 nm
D	Yes	Yes	480 nm

*Table 1 : List of samples*

### 3. RESULTS

To study the InGaN UL impact on the optical quality of the material, cathodoluminescence (CL) experiments were carried out at room temperature on a single NW from sample C, dispersed on a TEM copper/carbon grid, using an Allalin-type Attolight equipment. Hyperspectral mapping was achieved using an incident e-beam of 10kV/10nA.

Three spectra extracted from one hyperspectral mapping at room temperature of the single NW are shown in fig 1a). The location of the different layers in the NW are delineated in the SEM picture in fig 1c), along with the CL mapping superimposed to the NW SEM picture (fig 1b) in order to spatially determine the origin of the luminescence in the NW. Three CL emission bands appear at 365 nm (FWHM = 15nm), 390 nm (FWHM = 23 nm) and 615 nm (FWHM = 85nm). The 615 nm contribution matches with the InGaN/GaN MQWs position, while the 390 nm contribution coincides with the InGaN UL, consistent with a InN molar fraction of around 3%. Interestingly, the signal at 365 nm originates from the GaN spacer grown

above the UL. By contrast, only weak luminescence comes from the GaN section below the UL. In this case, the weak MQW contribution to the CL spectrum

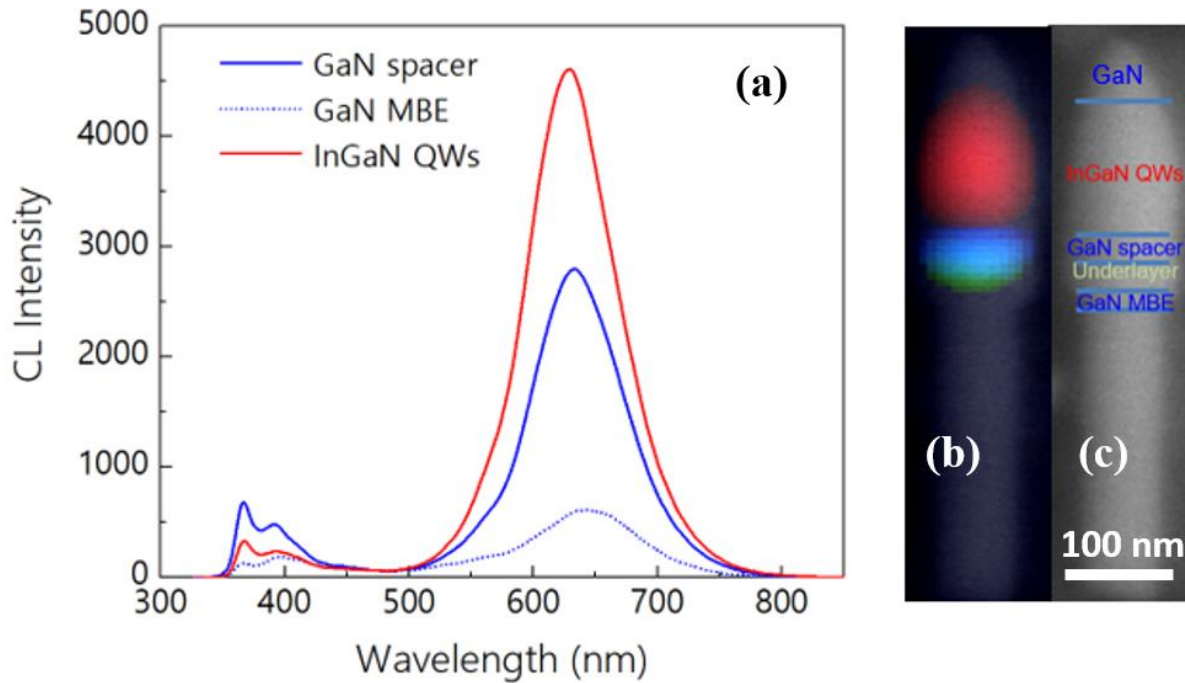


Fig 1. (a) Room temperature CL spectra extracted from the (b) hyperspectral mapping of a single NW (sample C). A SEM image is superposed to the mapping. The red, blue and green colors are assigned to the electron excitation mapping in the InGaN QWs, the GaN and the underlayer, respectively. (c) SEM image of the studied NW with the approximate location of the different layers in the NW deduced from CL mapping.

corresponds to excitation by the electrons retrodiffused by the copper/carbon grid. The weak luminescence of the 25 nm thick MBE-grown GaN section on the template is assigned to the likely presence of chemical impurities resulting from the transfer from MOCVD to MBE set-up.

In order to investigate the potential impact of the UL on the MQWs luminescence, we performed power dependent micro-photoluminescence (PD- $\mu$ PL)<sup>[6]</sup> experiments on sample A and on the reference, using a 405-nm laser as an excitation source. The laser spot diameter being around 3  $\mu$ m, about 15 NWs of 240-nm diameter were excited during the experiment. The

luminescence efficiency is defined as the integrated PL intensity divided by the excitation power density. As shown in figure 2a, the luminescence efficiency of the reference sample plotted as a function of excitation power density exhibits a plateau for increasing power density until a sharp decrease starting at  $10^5 \text{ W.cm}^{-2}$ . By contrast, sample A exhibits a higher luminescence efficiency whatever the excitation power density value, which directly shows the UL benefits. Moreover, the efficiency curve as a function of the excitation power exhibits a bell shape, allowing one to identify several regimes. In particular, we observe an increase (slope  $> 1$ ) of the luminescence efficiency starting at around  $1 \text{ W.cm}^{-2}$ . As in the case of the reference sample, the luminescence efficiency drastically decreases above  $10^5 \text{ W.cm}^{-2}$ . Furthermore, an extra set of PD- $\mu$ PL was performed on sample A, for three different diameter values: 180, 240 and 275 nm. The corresponding efficiency curves (fig. 2b) exhibit a bell-shape, confirming the results shown in fig 2a. Interestingly, one can notice a diameter dependence on the luminescence efficiency evolution. Indeed, for the full range of excitation power density, the luminescence efficiency is larger as the NWs diameter value decreases. Also, the maximum luminescence efficiency is reached at a higher excitation power density value when the NW diameter is larger, as a clue that the NRC density is reduced for NW with a small diameter and an UL.

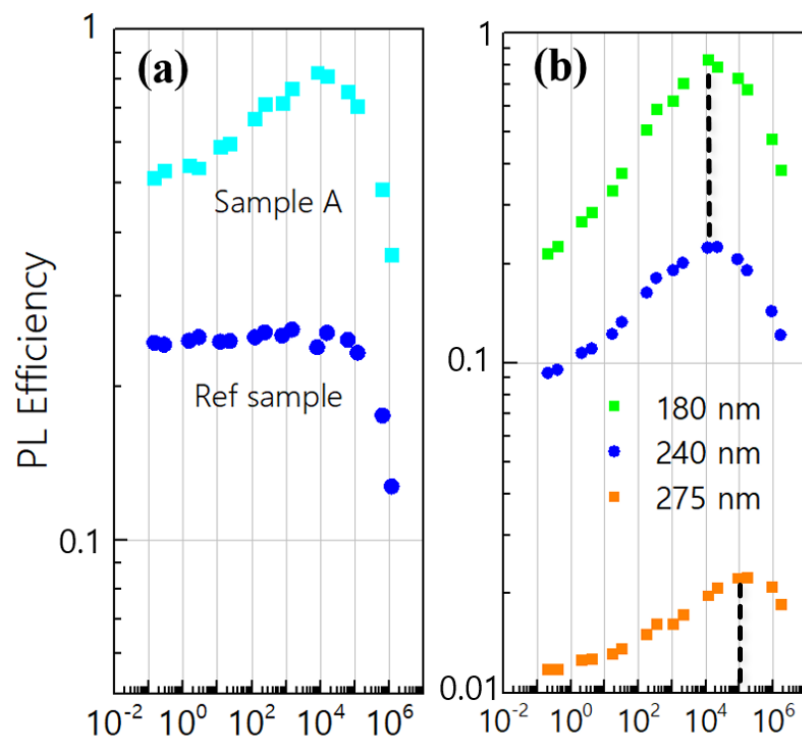


Fig 2. (a) Room temperature power dependent micro-PL experiments carried out for sample A (light blue) and a reference sample (dark blue). (b) Room temperature power dependent micro-PL experiments carried out for a sample with underlayer for three diameters values: 180, 240 and 275 nm. The dashed lines correspond to PL efficiency maximum.

The internal quantum efficiency, IQE, is often described in the frame of the ABC model:

$$\blacktriangleright IQE = \frac{Bn(n_0+n)}{An+Bn(n_0+n)+Cn^3}$$

where  $n$  is the generated carrier density,  $n_0$  the residual n-doping carrier density in the material, and  $A$ ,  $B$  and  $C$  the Shockley-Read-Hall (SRH) (non-radiative), radiative and Auger recombination coefficients, respectively. The limitations of this phenomenological model, which in general fails to account for the complexity of carrier recombination mechanism, have been recently reviewed by David et al<sup>30</sup>. Moreover, in the case of a population of size-dispersed NWs, NRC density variations from wire to wire, could result in a dispersion of  $A$  values at the scale of single NWs, making the ABC model irrelevant to describe their ensemble. However, despite these limitations, the ABC model has the virtue of providing a qualitative view of the recombination trends. In particular, in the low power density regime for which  $n \ll n_0$ , the plateau observed in absence of UL in figure 2a corresponds to a constant IQE equal to  $Bn_0/(A+Bn_0)$ , i.e. to a regime governed by both the non-radiative recombination and residual doping  $n_0$ . Clearly, the addition of an UL leads to an increased efficiency and to a departure from the linear regime, as an evidence that either the NRC density was reduced or the residual doping increased. However, these observations may also be the result of extraction and/or absorption effects, which will be discussed in the TR-PL section below. As the reference and sample A

were grown in similar experimental conditions, it can be reasonably assumed that their residual doping is likely the same. Then the supra-linear increase of PL intensity as a function of excitation power density can be tentatively assigned to the saturation of NRC-related recombination and increasing radiative recombination. For both samples, the sharp decrease of the luminescence efficiency at excitation power densities higher than  $10^5 \text{ W/cm}^2$  corresponds to Auger recombination, taking over the radiative recombination.

Additional time-resolved photoluminescence (TR-PL) experiments were performed at room temperature on sample A and on the reference, to investigate the effect of the UL on recombination dynamics in InGaN MQWs. The 405-nm second harmonic of a 76 MHz pulsed Ti:Al<sub>2</sub>O<sub>3</sub> laser output was used as an excitation source. During these measurements, about 15 NWs were excited under an average power density value of  $10^2 \text{ W.cm}^{-2}$ , in order to work in the regime where the radiative recombination is dominant. For each sample, the PL intensity was measured, and its time evolution plotted for three NW diameter values, namely 180, 240 and 275 nm (see fig 3). Recombination lifetimes were extracted using a single exponential fit at long delays, in order to avoid the influence of Auger recombination, are reported in Table 2).

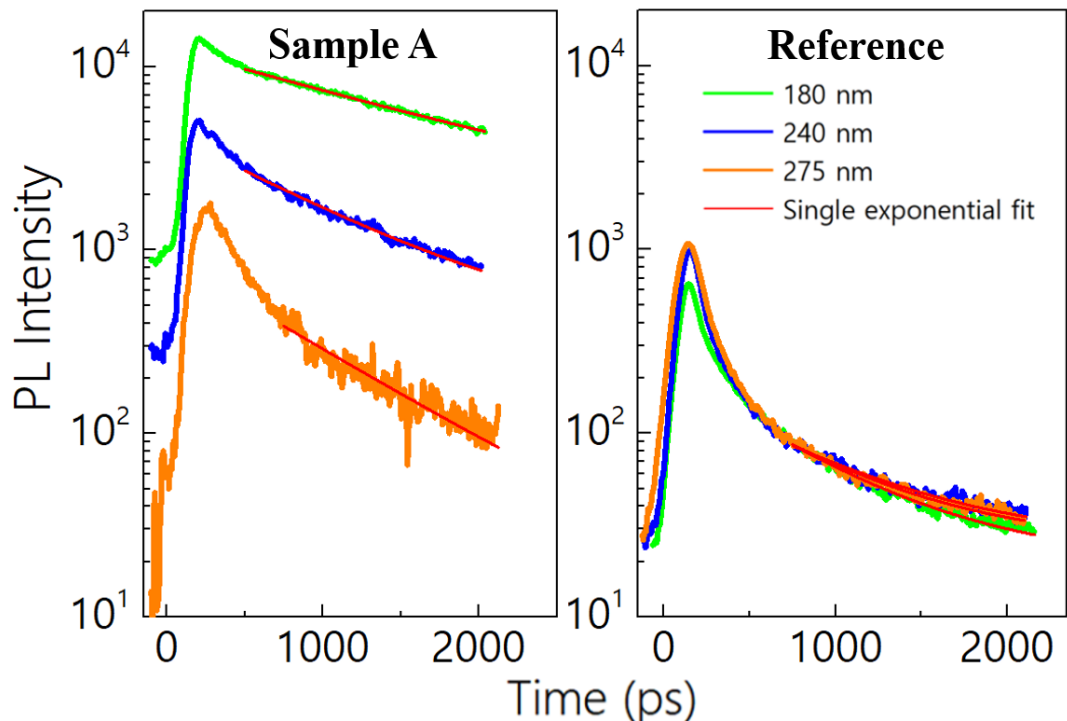


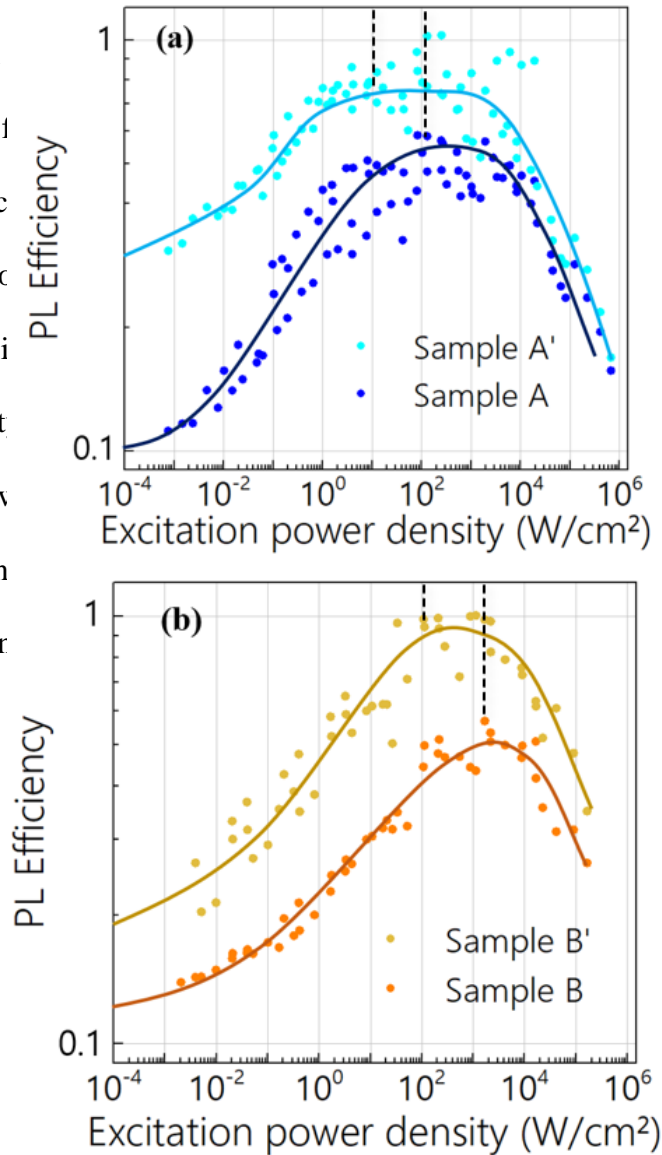
Fig 3. Room temperature TR-PL experiments performed for the reference sample and sample A. Measurements were performed for 3 different diameters values: 180 nm (green solid line), 240 nm (blue solid line) and 275 nm (orange solid line).

<b>Diameter (nm)</b>	<b>Effective lifetime (ns)</b>	
	<b>Reference</b>	<b>Sample A</b>
180	$0.66 \pm 0.006$	$1.6 \pm 0.007$
240	$0.68 \pm 0.007$	$0.89 \pm 0.006$
275	$0.75 \pm 0.011$	$0.70 \pm 0.013$

Table 2 : Recombination lifetimes for reference and sample A as a function of diameter

Noticeably maximum PL intensities for sample A are higher than for the reference one, whatever the NW diameter value, which is consistent with luminescence efficiency results in figure 2b. Moreover, the PL intensities of the reference sample display a similar time evolution for all diameters, assessed by similar effective lifetime values, suggesting that the NW diameter size does not significantly influence the recombination dynamics in this case. However, the opposite can be seen for sample A. In fact, one can notice that the maximum PL intensity is larger for smaller NW diameter. Similarly, the lower the NW diameter, the longer the effective lifetime is. The effective lifetime being independent of extraction effects, these results, consistent with the PD- $\mu$ PL measurements in fig 2b), cannot be only attributed to a change in light absorption and/or extraction efficiency. Moreover, as the surface/volume ratio is increasing for decreasing NW diameter, they suggest that either NR surface recombination is not primarily dominating the carrier dynamics, in line with the results of Hauswald et al concerning GaN NWs<sup>31</sup>, and/or that the NRC concentration is lower in small diameter NWs. To test these hypotheses, an aluminium oxide (AlO<sub>x</sub>) layer was deposited on sample A by Atomic Layer Deposition (ALD) technique. Then, a new set of PD- $\mu$ PL experiments was

performed on this new sample A' under the same previous conditions. The comparison of 140-nm NWs diameter from curves are presented in measured emission efficiency is tentatively assigned to of the passivating layer i at the same power density difference appears at low AlO<sub>x</sub> deposition is sign easing defect saturation recombination channel.



tion power density  
 · density range, the  
 than before, which  
 active index  $n_{\text{AlO}_x}$ ,  
 s become effective  
 ntrast, a significant  
 ion efficiency after  
 face passivation is  
 sion of a surface

Fig 4. Power dependent micro-PL measurements acquired before and after the aluminium oxide layer deposition for samples emitting at (a) 480 nm and (b) 590 nm. Solid lines are guides to the eye. The dashed lines correspond to the onset of saturation.

In a next step, we investigated the consequences of surface passivation in the case of InGaN MQWs with a higher In content. To this end, PD- $\mu$ PL measurements were performed on 140-nm NWs diameter from sample B. After the deposition of an AlO<sub>x</sub> layer, an extra set of PD- $\mu$ PL experiments were performed on that new sample B'. The emission efficiency vs excitation power densities curves are plotted in fig 4b. By comparison with sample A, the maximum efficiency for sample B is reached for about two orders of magnitude larger excitation power density ( $10^3$  vs  $10^1$  W.cm<sup>-2</sup>), suggesting that NRC density is increasing with In content. The emission efficiency measured after surface passivation is about 80% higher at the plateau than before, whatever the excitation power density. In the same way, the Auger losses become effective at the same power density ( $10^4$  W/cm<sup>2</sup>) in both cases.. Moreover, no significant differences of luminescence intensity come up at low power excitation density between B and B', as a clue, on the one hand, that surface recombination is not dominant and emphasizing the presence of an extra source of NRCs. However, on the other hand, the maximum efficiency for sample B' is reached for an excitation power density one decade less than for sample B ( $10^2$  W/cm<sup>2</sup> vs  $10^3$  W/cm<sup>2</sup>) suggesting that surface recombination, even if not being the dominant non radiative recombination channel, is present and can be reduced by the AlO<sub>x</sub> layer deposition

With the aim of unravelling the impact of diameter on luminescence efficiency at the nanoscale, CL mapping experiments of single NWs were performed on sample A', for the three different NW diameters studied before. The spacing between the NWs is 400 nm. The voltage acceleration was set to 5 kV. For each diameter, top-view CL mappings of 500 NWs were acquired at room temperature and are presented in fig 5a, 5b and 5c. Interestingly, as shown in inset in fig 5a, 5b and 5c, the luminescence is homogeneous for the 180 nm [g3]diameter, whereas a luminescent ring surrounding a less luminescent central part is identified for the 240 and 275 nm diameters. The CL spectra plotted in fig 5d are acquired in the side and the centre of a NW, confirming that the CL intensity in the ring is two times higher than in the centre part. Remarkably, no wavelength shift from center to ring is observed, discarding the hypothesis that the ring could result from the growth of QWs with a lower In content on semipolar facets<sup>32,33</sup>.

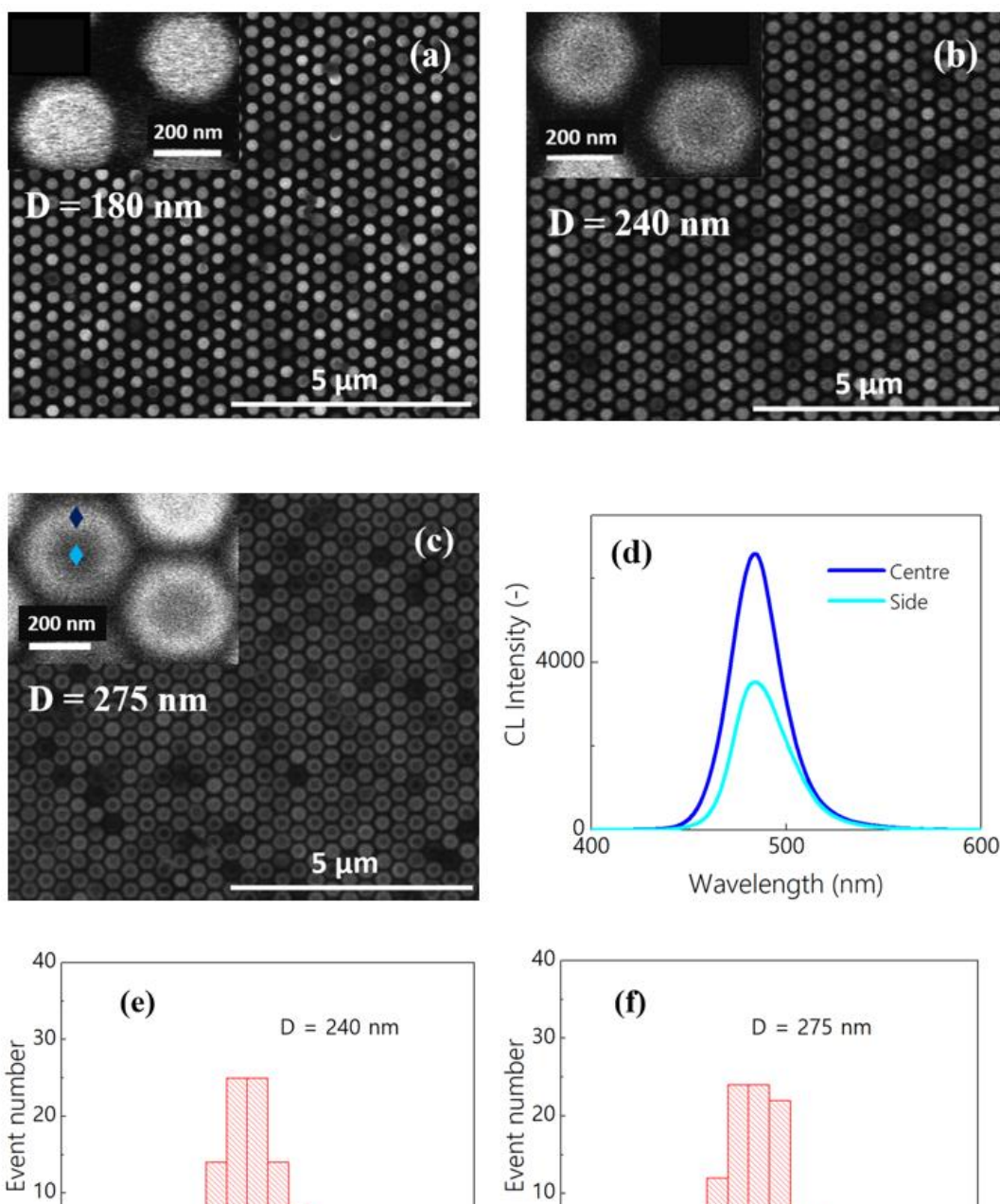


Fig 5. (a-c) Top view CL mappings of 500 NWs, for 180, 240 and 275-nm NWs diameter, respectively for sample A'. The insets show a top-view CL intensity of 2 NWs, for 180, 240 and 275-nm diameter, respectively. (d) CL spectra of the side and the centre for one NW from sample A'. (e, f) Luminescence ring width distribution for 240 and 275 nm NW diameter.

A statistical analysis of the luminescent ring width was performed on about 100 NWs for the 240 and 275 nm diameter values. The resulting distributions are plotted in figure 5e and 5f. The average ring width is 90 nm for both diameters, as a clue that the physical phenomenon responsible for the ring formation has a common origin in both cases. Accordingly, the homogeneous luminescence observed for the smallest NW diameter, is assigned to the fact that their diameter value is lower than twice the ring width.

In order to be able to link the CL efficiency drop at the center of the large wires to a change of NRC density, we then used spatially resolved time-correlated cathodoluminescence (TC-CL) spectroscopy<sup>34</sup>. The measurement was achieved using an incident e-beam of 5kV/10 pA. The extracted CL lifetime profile along the diameter of a ring-exhibiting NW is shown in figure 6. Interestingly, this profile puts in evidence longer lifetime values in periphery, i.e. in the ring, than in the centre of the NW, as a further clue of a lower density of NRCs in the ring area.

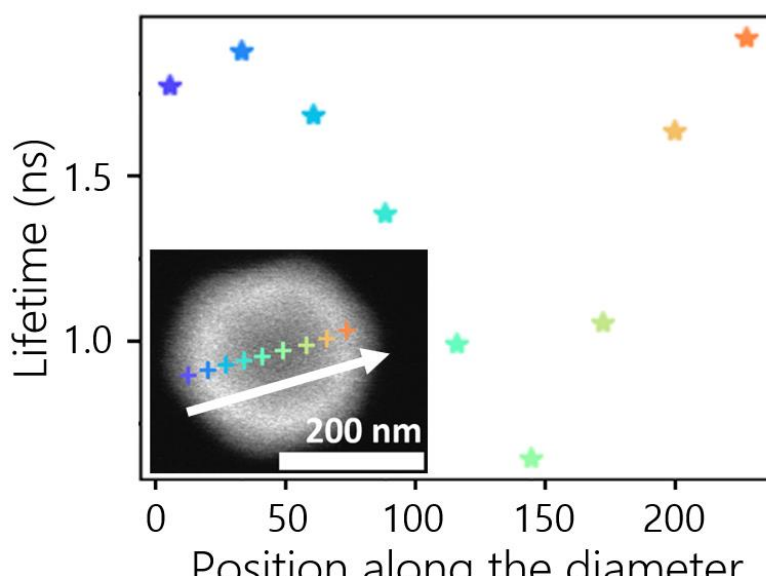


Fig 6. CL lifetime values along the diameter for a 275 nm diameter NW from sample A'.

In order to get more insight in the formation mechanism of the NRCs responsible for the above features, both the influence of NW array pitch and growth rate on the luminescence of the NWs were examined. As concerns pitch, an extra CL-mapping was acquired at room temperature for 180-nm diameter NWs from another area of sample A'. In this area, the NW spacing was 200 nm. [AC4]One can notice in figure 7a the presence of an inhomogeneous luminescence at the NW scale, namely a luminescent ring surrounding a less-luminescent centre. A statistical analysis of the luminescent ring width was performed on about 100 NWs from this CL mapping. The resulting distribution is plotted in figure 7b. The average ring width is 50 nm. By comparison with the CL mapping in fig 5a where the 180-nm NWs diameter exhibits an homogeneous luminescence, these results suggests that the pitch reduction leads to an increased NRC density in the NW central part, concomitantly with the formation of a thinner luminescent ring in periphery.

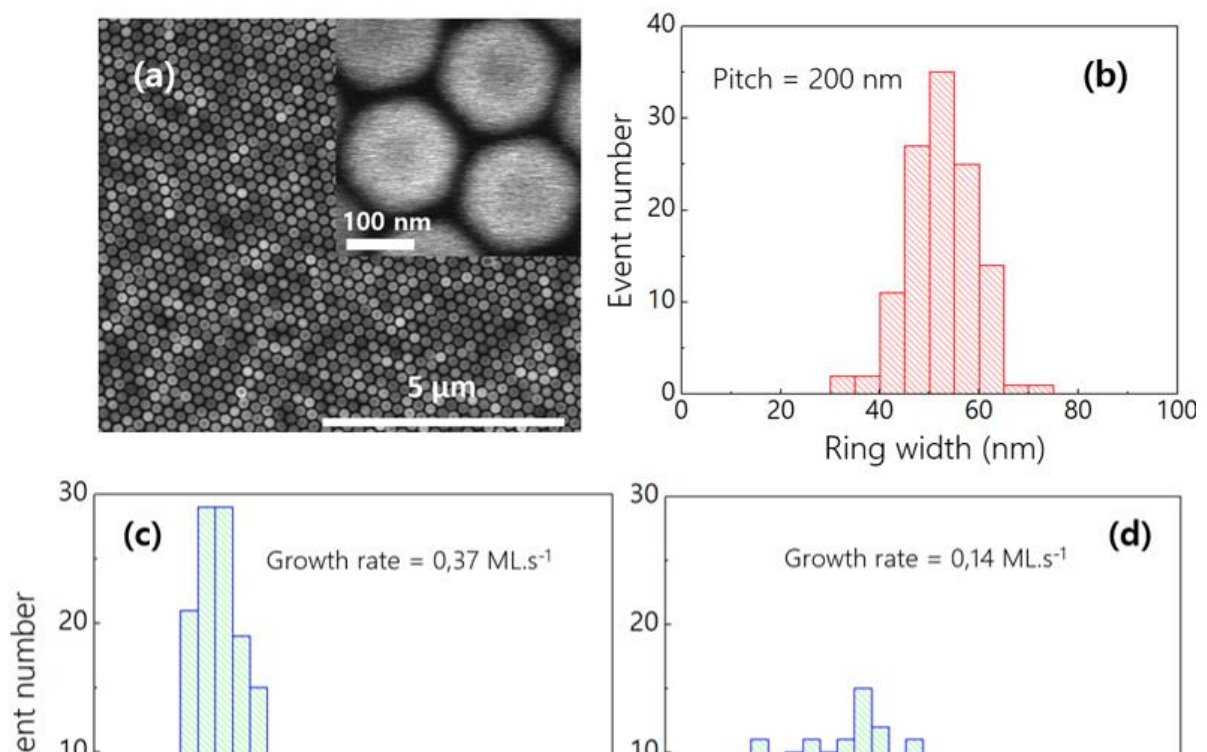


Fig 7. (a) Top view CL mappings of about 500 NWs, for 180-nm NWs diameter. The inset shows a top-view CL intensity of 3 NWs of 180-nm diameter. (b) Luminescence ring width distribution for 180-nm NWs diameter separated by a 200-nm pitch. (c-d) CL Intensity distribution for 240-nm NW diameter from sample A' and D grown at (c) 0,37 ML.s<sup>-1</sup> and (d) 0,14 ML.s<sup>-1</sup> respectively.

As concerns the NW growth rate, figure 7c and 7d show the CL intensity histogram of samples A and D, respectively. Interestingly, it appears that the average intensity for sample D (about 6000 counts) is significantly shifted towards higher intensities, to be compared to about 3000 counts for sample A', suggesting that a lower growth rate either reduces the NRC formation rate or favours their curing, as it will be further discussed.

#### 4. DISCUSSION

The enhancement of the emission efficiency in the MBE-grown GaN section above the UL points towards NRC transferred from the MOCVD-grown GaN NW template into the MBE-grown GaN section below the UL and supports the assumption that the UL trapped a fraction of the total number of those NRCs. In absence of extended crystalline defects such as dislocations in NWs, the major source of NRCs is expected to consist of extrinsic point defects such as Fe, C or complexes associating Ga and nitrogen vacancies,  $V_{Ga}$  and  $V_N$ <sup>35</sup>. Accordingly, Point defects formed during the MOCVD growth of the GaN NW template and accumulating at the surface<sup>36</sup> could be a candidate to account for the lack of luminescence in the MOCVD-grown NW template. In this scenario, these NRCs can be transferred into the MBE-grown GaN

section and further trapped in the InGaN UL grown onto it. Similar to the case of MOCVD layers, the point defect trapping by the UL should occur through the creation of In-point defect complexes, preventing their further segregation in GaN spacer and InGaN QWs.

While clearly supporting the beneficial effect of the UL to decrease the total density of NRCs with respect to the reference sample, the PD- $\mu$ PL data also suggest that surface states, unidentified chemical impurities and/or residual point defect are not fully suppressed. This statement is supported on the one hand by the effect of ALD passivation at low excitation power observed for samples A and A', which reveals the presence of surface states. However, on the other hand, the higher luminescence intensity observed for smaller diameters in sample A rather suggests that another type of NRCs, the number of which decreases with diameter is affecting the MQWs luminescence intensity.

Chemical impurities such as O associated with Ga vacancies<sup>37</sup>, or Ca<sup>38</sup> currently invoked to account for non-radiative recombination are unlikely candidates to account for this feature. In particular, there is no reason to believe that they should be incorporated preferentially in the *central part* of the heterostructure, as suggested by the TC-CL data shown in figure 6. Moreover, if considering a constant flux of chemical impurities only dependent on the MBE chamber base vacuum, one should expect a larger amount of incorporated impurities for lower growth rate, contrary to results shown in figure 7c. These results suggest that the NRCs responsible for this behaviour could be of intrinsic origin rather than extrinsic. Also, the pitch variation, which has a clear influence on the luminescence properties of the NWs, should not affect the incorporation rate of these chemical impurities in the NWs. Alternatively,  $V_{Ga}$  or residual  $V_N$  untrapped in the UL or  $V_N$  incorporated during the growth of the MQWs themselves could be a candidate to account for the overall limited PL efficiency of InGaN/GaN NW heterostructures. As concerns  $V_N$ , it has to be reminded that they can easily form at the surface of GaN during growth. This also holds in the case of InGaN for which the  $V_N$  energy formation

is found to decrease for increasing InN molar fraction<sup>28</sup>. The  $V_N$  formation at the surface of InGaN/GaN NW heterostructures is expected to be furthermore eased when using PA-MBE growth technique, as it is known that the continuous exposure of the growing surface to a flux of neutral N and charged species with a large kinetic energy favours the formation of  $V_N$  at the surface of GaN and InGaN<sup>39</sup>. The  $V_N$  formation rate is expected to be even larger in the case of InGaN, which is grown at a temperature close to the decomposition temperature. However, besides limiting the formation of  $V_{Ga}$  or  $V_{In}$ , metal excess is expected to stabilize N adatoms and prevent them from recombining into  $N_2$  and desorbing from the surface where  $V_N$  should be left<sup>40</sup>. It is then possible that the metal excess diffusing from the sidewalls towards the NW top and accumulating in the NW periphery<sup>41,42</sup> results in N stabilization and reduced  $V_N$  formation probability. The data shown in figure 7 demonstrate that the shadowing effect, induced by the pitch reduction, causes a diminution of the ring width. Accordingly, this feature is tentatively assigned to a reduction of metal flux diffusing from the side walls associated with a limitation of metal excess on top, which could affect metal-assisted N stabilization and increase the  $V_N$  formation probability. However, the metal excess in NW periphery and its dependence on pitch value could equally result in a decrease in  $V_{Ga}$  or  $V_{In}$  formation rate, preventing at this stage a firm conclusion on the nature of the NRCs formed during the growth of the InGaN MQW heterostructure but definitely pointing towards an intrinsic origin.

## 5. CONCLUSION

In conclusion, our data demonstrate that the luminescence of the InGaN/GaN NW heterostructures under study is limited by both surface recombination and at least another kind of NRCs. Moreover, the relative importance of both contributions is depending on the diameter of the heterostructures and on the InN molar fraction, with an increasing influence of NRCs for increasing InN molar fraction. On the basis of data from CL, PL and TR-PL measurements, we

showed that the addition of an InGaN UL with a low In content enhances the luminescence efficiency of NW-based InGaN/GaN MQWs elaborated by MBE, consistent with the effectiveness of a  $V_N$  trapping mechanism. While most point defects present in the MOCVD NW template are thus prevented to migrate into the upper MBE-grown section, the presence of an additional source of NRCs likely formed during the growth of InGaN/GaN MQWs was identified. Our experimental CL data strongly suggest they are of intrinsic origin and could be  $V_{Ga}$ ,  $V_{In}$  or  $V_N$  generated during PA-MBE growth. Non radiative recombination associated with these defects is prevailing over surface non radiative recombination for increasing InN molar fraction and could account for the decreasing luminescence efficiency observed in the long wavelength emission range. In practice our results are assessing the counter-intuitive prediction that small diameter NW-based LEDs are preferable for optimized efficiency.

**ACKNOWLEDGMENTS** We acknowledge the help of Y. Curé and F. Jourdan for technical support in the MBE experiments and of N. Rochat for her assistance in CL experiments. We thank Dr B. Gayral for fruitful discussions and careful reading of the manuscript.

## REFERENCES

- (1) Hurni, C. A.; David, A.; Cich, M. J.; Aldaz, R. I.; Ellis, B.; Huang, K.; Tyagi, A.; DeLille, R. A.; Craven, M. D.; Steranka, F. M.; Krames, M. R. Bulk GaN Flip-Chip Violet Light-Emitting Diodes with Optimized Efficiency for High-Power Operation. *Appl. Phys. Lett.* **2015**, *106* (3), 031101. <https://doi.org/10.1063/1.4905873>.
- (2) Wierer, J. J.; Tansu, N. III-Nitride Micro-LEDs for Efficient Emissive Displays. *Laser Photonics Rev.* **2019**, *13* (9), 1900141. <https://doi.org/10.1002/lpor.201900141>.
- (3) Lin, J. Y.; Jiang, H. X. Development of MicroLED. *Appl. Phys. Lett.* **2020**, *116* (10), 100502. <https://doi.org/10.1063/1.5145201>.
- (4) Templier, F. GaN-Based Emissive Microdisplays: A Very Promising Technology for Compact, Ultra-High Brightness Display Systems: GaN-Based Emissive

- Microdisplays. *J. Soc. Inf. Disp.* **2016**, *24* (11), 669–675.  
<https://doi.org/10.1002/jsid.516>.
- (5) Jiang, H. X.; Jin, S. X.; Li, J.; Shakya, J.; Lin, J. Y. III-Nitride Blue Microdisplays. *Appl. Phys. Lett.* **2001**, *78* (9), 1303–1305. <https://doi.org/10.1063/1.1351521>.
  - (6) Pelá, R. R.; Caetano, C.; Marques, M.; Ferreira, L. G.; Furthmüller, J.; Teles, L. K. Accurate Band Gaps of AlGa<sub>N</sub>, InGa<sub>N</sub>, and AlIn<sub>N</sub> Alloys Calculations Based on LDA-1/2 Approach. *Appl. Phys. Lett.* **2011**, *98* (15), 151907.  
<https://doi.org/10.1063/1.3576570>.
  - (7) Mukai, T.; Yamada, M.; Nakamura, S. Characteristics of InGa<sub>N</sub>-Based UV/Blue/Green/Amber/Red Light-Emitting Diodes. *Jpn. J. Appl. Phys.* **1999**, *38* (Part 1, No. 7A), 3976–3981. <https://doi.org/10.1143/JJAP.38.3976>.
  - (8) Liu, X.; Sun, Y.; Malhotra, Y.; Pandey, A.; Wu, Y.; Sun, K.; Mi, Z. High Efficiency InGa<sub>N</sub> Nanowire Tunnel Junction Green Micro-LEDs. *Appl. Phys. Lett.* **2021**, *119* (14), 141110. <https://doi.org/10.1063/5.0059701>.
  - (9) Kishino, K.; Sakakibara, N.; Narita, K.; Oto, T. Two-Dimensional Multicolor (RGBY) Integrated Nanocolumn Micro-LEDs as a Fundamental Technology of Micro-LED Display. *Appl. Phys. Express* **2020**, *13* (1), 014003. <https://doi.org/10.7567/1882-0786/ab5ad3>.
  - (10) Nami, M.; Rashidi, A.; Monavarian, M.; Mishkat-UI-Masabih, S.; Rishinaramangalam, Ashwin. K.; Brueck, S. R. J.; Feezell, D. Electrically Injected GHz-Class Ga<sub>N</sub>/InGa<sub>N</sub> Core–Shell Nanowire-Based MLEDs: Carrier Dynamics and Nanoscale Homogeneity. *ACS Photonics* **2019**, *6* (7), 1618–1625. <https://doi.org/10.1021/acsp Photonics.9b00639>.
  - (11) Glas, F. Critical Dimensions for the Plastic Relaxation of Strained Axial Heterostructures in Free-Standing Nanowires. *Phys. Rev. B* **2006**, *74* (12), 121302.  
<https://doi.org/10.1103/PhysRevB.74.121302>.
  - (12) Landré, O.; Camacho, D.; Bougerol, C.; Niquet, Y. M.; Favre-Nicolin, V.; Renaud, G.; Renevier, H.; Daudin, B. Elastic Strain Relaxation in Ga<sub>N</sub>/Al<sub>N</sub> Nanowire Superlattice. *Phys. Rev. B* **2010**, *81* (15), 153306. <https://doi.org/10.1103/PhysRevB.81.153306>.
  - (13) Yoshizawa, M.; Kikuchi, A.; Mori, M.; Fujita, N.; Kishino, K. Growth of Self-Organized Ga<sub>N</sub> Nanostructures on Al<sub>2</sub>O<sub>3</sub>(0001) by RF-Radical Source Molecular Beam Epitaxy. *Jpn. J. Appl. Phys.* **1997**, *36*, 459–462.
  - (14) Yoshizawa, M.; Kikuchi, A.; Fujita, N.; Kushi, K.; Sasamoto, H.; Kishino, K. Self-Organization of Ga<sub>N</sub>/Al<sub>0.18</sub>Ga<sub>0.82</sub>N Multi-Layer Nano-Columns on (0001) Al<sub>2</sub>O<sub>3</sub> by RF Molecular Beam Epitaxy for Fabricating Ga<sub>N</sub> Quantum Disks. *J. Cryst. Growth* **1998**, *189/190*, 138–141.
  - (15) Sanchez-Garcia, M. A.; Calleja, E.; Monroy, E.; Sanchez, F. J.; Calle, F.; Muñoz, E.; Beresford, R. The Effect of the III/V Ratio and Substrate Temperature on the Morphology and Properties of Ga<sub>N</sub>- and Al<sub>N</sub>-Layers Grown by Molecular Beam Epitaxy on Si(1 1 1). *J. Cryst. Growth* **1998**, *183* (1–2), 23–30.  
[https://doi.org/10.1016/S0022-0248\(97\)00386-2](https://doi.org/10.1016/S0022-0248(97)00386-2).
  - (16) Calleja, E.; Sánchez-García, M. A.; Sánchez, F. J.; Calle, F.; Naranjo, F. B.; Muñoz, E.; Molina, S. I.; Sánchez, A. M.; Pacheco, F. J.; García, R. Growth of III-Nitrides on Si(111) by Molecular Beam Epitaxy Doping, Optical, and Electrical Properties. *J. Cryst. Growth* **1999**, *201–202*, 296–317. [https://doi.org/10.1016/S0022-0248\(98\)01346-3](https://doi.org/10.1016/S0022-0248(98)01346-3).
  - (17) Sugahara, T.; Sato, H.; Hao, M.; Naoi, Y.; Kurai, S.; Tottori, S.; Yamashita, K.; Nishino, K.; Romano, L. T.; Sakai, S. Direct Evidence That Dislocations Are Non-Radiative Recombination Centers in Ga<sub>N</sub>. *Jpn. J. Appl. Phys.* **1998**, *37* (Part 2, No. 4A), L398–L400. <https://doi.org/10.1143/JJAP.37.L398>.

- (18) Abell, J.; Moustakas, T. D. The Role of Dislocations as Nonradiative Recombination Centers in InGaN Quantum Wells. *Appl. Phys. Lett.* **2008**, *92* (9), 091901. <https://doi.org/10.1063/1.2889444>.
- (19) Corfdir, P.; Lefebvre, P.; Ristić, J.; Valvin, P.; Calleja, E.; Trampert, A.; Ganière, J.-D.; Deveaud-Plédran, B. Time-Resolved Spectroscopy on GaN Nanocolumns Grown by Plasma Assisted Molecular Beam Epitaxy on Si Substrates. *J. Appl. Phys.* **2009**, *105* (1), 013113. <https://doi.org/10.1063/1.3062742>.
- (20) Gorgis, A.; Flissikowski, T.; Brandt, O.; Chèze, C.; Geelhaar, L.; Riechert, H.; Grahn, H. T. Time-Resolved Photoluminescence Spectroscopy of Individual GaN Nanowires. *Phys. Rev. B* **2012**, *86* (4), 041302. <https://doi.org/10.1103/PhysRevB.86.041302>.
- (21) Chichibu, S. F.; Uedono, A.; Onuma, T.; Sota, T.; Haskell, B. A.; DenBaars, S. P.; Speck, J. S.; Nakamura, S. Limiting Factors of Room-Temperature Nonradiative Photoluminescence Lifetime in Polar and Nonpolar GaN Studied by Time-Resolved Photoluminescence and Slow Positron Annihilation Techniques. *Appl. Phys. Lett.* **2005**, *86* (2), 021914. <https://doi.org/10.1063/1.1851619>.
- (22) Armstrong, A. M.; Crawford, M. H.; Koleske, D. D. Contribution of Deep-Level Defects to Decreasing Radiative Efficiency of InGaN/GaN Quantum Wells with Increasing Emission Wavelength. *Appl. Phys. Express* **2014**, *7* (3), 032101. <https://doi.org/10.7567/APEX.7.032101>.
- (23) Haller, C.; Carlin, J.-F.; Jacopin, G.; Martin, D.; Butté, R.; Grandjean, N. Burying Non-Radiative Defects in InGaN Underlayer to Increase InGaN/GaN Quantum Well Efficiency. *Appl. Phys. Lett.* **2017**, *111* (26), 262101. <https://doi.org/10.1063/1.5007616>.
- (24) Haller, C.; Carlin, J.-F.; Jacopin, G.; Liu, W.; Martin, D.; Butté, R.; Grandjean, N. GaN Surface as the Source of Non-Radiative Defects in InGaN/GaN Quantum Wells. *Appl. Phys. Lett.* **2018**, *113* (11), 111106. <https://doi.org/10.1063/1.5048010>.
- (25) Armstrong, A. M.; Bryant, B. N.; Crawford, M. H.; Koleske, D. D.; Lee, S. R.; Wierer, J. J. Defect-Reduction Mechanism for Improving Radiative Efficiency in InGaN/GaN Light-Emitting Diodes Using InGaN Underlayers. *J. Appl. Phys.* **2015**, *117* (13), 134501. <https://doi.org/10.1063/1.4916727>.
- (26) Akasaka, T.; Gotoh, H.; Saito, T.; Makimoto, T. High Luminescent Efficiency of InGaN Multiple Quantum Wells Grown on InGaN Underlying Layers. *Appl. Phys. Lett.* **2004**, *85* (15), 3089–3091. <https://doi.org/10.1063/1.1804607>.
- (27) Weatherley, T. F. K.; Liu, W.; Osokin, V.; Alexander, D. T. L.; Taylor, R. A.; Carlin, J.-F.; Butté, R.; Grandjean, N. Imaging Nonradiative Point Defects Buried in Quantum Wells Using Cathodoluminescence. *Nano Lett.* **2021**, *21* (12), 5217–5224. <https://doi.org/10.1021/acs.nanolett.1c01295>.
- (28) Bezyazychnaya, T. V.; Kabanau, D. M.; Kabanov, V. V.; Lebiadok, Y. V.; Ryabtsev, A. G.; Ryabtsev, G. I.; Zelenkovskii, V. M.; Mehta, S. K. Influence of Vacancies on Indium Atom Distribution in InGaAs and InGaN Compounds. *Lith. J. Phys.* **2015**, *55* (1). <https://doi.org/10.3952/physics.v55i1.3053>.
- (29) Uedono, A.; Watanabe, T.; Kimura, S.; Zhang, Y.; Lozac'h, M.; Sang, L.; Ishibashi, S.; Oshima, N.; Suzuki, R.; Sumiya, M. Vacancy-Type Defects in In<sub>x</sub>Ga<sub>1-x</sub>N Grown on GaN Templates Probed Using Monoenergetic Positron Beams. *J. Appl. Phys.* **2013**, *114* (18), 184504. <https://doi.org/10.1063/1.4830033>.
- (30) David, A.; Young, N. G.; Lund, C.; Craven, M. D. Review—The Physics of Recombinations in III-Nitride Emitters. *ECS J. Solid State Sci. Technol.* **2020**, *9* (1), 016021. <https://doi.org/10.1149/2.0372001JSS>.
- (31) Hauswald, C.; Corfdir, P.; Zettler, J. K.; Kaganer, V. M.; Sabelfeld, K. K.; Fernández-Garrido, S.; Flissikowski, T.; Consonni, V.; Gotschke, T.; Grahn, H. T.; Geelhaar, L.;

- Brandt, O. Origin of the Nonradiative Decay of Bound Excitons in GaN Nanowires. *Phys. Rev. B* **2014**, *90* (16), 165304. <https://doi.org/10.1103/PhysRevB.90.165304>.
- (32) Kishino, K.; Yamano, K. Green-Light Nanocolumn Light Emitting Diodes With Triangular-Lattice Uniform Arrays of InGaN-Based Nanocolumns. *IEEE J. Quantum Electron.* **2014**, *50* (7), 538–547. <https://doi.org/10.1109/JQE.2014.2325013>.
- (33) Browne, D. A.; Young, E. C.; Lang, J. R.; Hurni, C. A.; Speck, J. S. Indium and Impurity Incorporation in InGaN Films on Polar, Nonpolar, and Semipolar GaN Orientations Grown by Ammonia Molecular Beam Epitaxy. *J. Vac. Sci. Technol. Vac. Surf. Films* **2012**, *30* (4), 041513. <https://doi.org/10.1116/1.4727967>.
- (34) Finot, S.; Le Maoult, C.; Gheeraert, E.; Vaufrey, D.; Jacopin, G. Surface Recombinations in III-Nitride Micro-LEDs Probed by Photon-Correlation Cathodoluminescence. *ACS Photonics* **2022**, *9* (1), 173–178. <https://doi.org/10.1021/acsp Photonics.1c01339>.
- (35) Chichibu, S. F.; Uedono, A.; Kojima, K.; Ikeda, H.; Fujito, K.; Takashima, S.; Edo, M.; Ueno, K.; Ishibashi, S. The Origins and Properties of Intrinsic Nonradiative Recombination Centers in Wide Bandgap GaN and AlGaIn. *J. Appl. Phys.* **2018**, *123* (16), 161413. <https://doi.org/10.1063/1.5012994>.
- (36) Chen, Y.; Haller, C.; Liu, W.; Karpov, S. Y.; Carlin, J.-F.; Grandjean, N. GaN Buffer Growth Temperature and Efficiency of InGaIn/GaN Quantum Wells: The Critical Role of Nitrogen Vacancies at the GaN Surface. *Appl. Phys. Lett.* **2021**, *118* (11), 111102. <https://doi.org/10.1063/5.0040326>.
- (37) Dreyer, C. E.; Alkauskas, A.; Lyons, J. L.; Speck, J. S.; Van de Walle, C. G. Gallium Vacancy Complexes as a Cause of Shockley-Read-Hall Recombination in III-Nitride Light Emitters. *Appl. Phys. Lett.* **2016**, *108* (14), 141101. <https://doi.org/10.1063/1.4942674>.
- (38) Young, E. C.; Grandjean, N.; Mates, T. E.; Speck, J. S. Calcium Impurity as a Source of Non-Radiative Recombination in (In,Ga)N Layers Grown by Molecular Beam Epitaxy. *Appl. Phys. Lett.* **2016**, *109* (21), 212103. <https://doi.org/10.1063/1.4968586>.
- (39) Fu, T. C.; Newman, N.; Jones, E.; Chan, J. S.; Liu, X.; Rubin, M. D.; Cheung, N. W.; Weber, E. R. The Influence of Nitrogen Ion Energy on the Quality of GaN Films Grown with Molecular Beam Epitaxy. *J. Electron. Mater.* **1995**, *24* (4), 249–255. <https://doi.org/10.1007/BF02659683>.
- (40) Zywietz, T.; Neugebauer, J.; Scheffler, M. Adatom Diffusion at GaN (0001) and (000 $\bar{1}$ ) Surfaces. *Appl. Phys. Lett.* **1998**, *73* (4), 487–489. <https://doi.org/10.1063/1.121909>.
- (41) Gruart, M.; Jacopin, G.; Daudin, B. Role of Ga Surface Diffusion in the Elongation Mechanism and Optical Properties of Catalyst-Free GaN Nanowires Grown by Molecular Beam Epitaxy. *Nano Lett.* **2019**, *19* (7), 4250–4256. <https://doi.org/10.1021/acsnanolett.9b00023>.
- (42) van Treeck, D.; Fernández-Garrido, S.; Geelhaar, L. Influence of the Source Arrangement on Shell Growth around GaN Nanowires in Molecular Beam Epitaxy. *Phys. Rev. Mater.* **2020**, *4* (1), 013404. <https://doi.org/10.1103/PhysRevMaterials.4.013404>.
- (43) Limpijumnong, S.; Van de Walle, C. Diffusivity of Native Defects in GaN. *Phys. Rev. B* **2004**, *69* (3), 035207. <https://doi.org/10.1103/PhysRevB.69.035207>.